I-1847c DR-0661-0

ornl

ORNL/TM-9183

NOTICE
PORTIONS OF THIS REPORT ARE ILLEGIBLE.
It has been reproduced from the best available copy to permit the broadest possible availability.

OAK RIDGE NATIONAL LABORATORY

MARTIN MARIETTA

A Numerical Model for Swirl Flow Cooling in High-Heat-Flux Particle Beam Targets and the Design of a Swirl-Flow-Based Plasma Limiter

S. L. Milora
S. K. Combs
C. A. Foster

MASTER

OPERATED BY
MARTIN MARIETTA ENERGY SYSTEMS, INC.
FOR THE UNITED STATES
DEPARTMENT OF ENERGY

ORNL/TM--9163

DE85 003824

Fusion Energy Division

A NUMERICAL MODEL FOR SWIRL FLOW COOLING IN HIGH-HEAT-FLUX PARTICLE BEAM TARGETS AND THE DESIGN OF A SWIRL-FLOW-BASED PLASMA LIMITER

S. L. Milora
S. K. Combs
C. A. Foster

Date Published - November 1984

Prepared by the
OAK RIDGE NATIONAL LABORATORY
Oak Ridge, Tennessee 37831
operated by
MARTIN MARIETTA ENERGY SYSTEMS, INC.
for the
U.S DEPARTMENT OF ENERGY
under Contract No. DE-AC05-840R21400

CONTENTS

ABSTRACT

An unsteady, two-dimensional heat conduction code has been used to study the performance of swirl-flow-based neutral particle beam targets. The model includes the effects of two-phase heat transfer and asymmetric heating of tubular elements. The calorimeter installed in the Medium Energy Test Facility, which has been subjected to 30-s neutral beam pulses with incident heat flux intensities of ≥ 5 kW/cm^2, has been modeled. The numerical results indicate that local heat fluxes in excess of 7 kW/cm^2 occur at the water-cooled surface on the side exposed to the beam. This exceeds critical heat flux limits for uniformly heated tubes with straight flow by approximately a factor of 5. The design of a plasma limiter based on swirl flow heat transfer is presented.

1. INTRODUCTION

High-heat-flux particle beam targets and calorimeters based on swirl flow heat transfer in tubular elements have been developed at Oak Ridge National Laboratory (ORNL). As described by Combs,[1] these compact, inexpensive components operate in a steady state at incident heat fluxes in excess of 5 kW/cm^2. The calorimeter installed on the ORNL Medium Energy Test Facility (METF) has absorbed an estimated 25,000 full-power ($\approx$3-MW) pulses for a cumulative ~70,000 beam seconds without failure.

It has long been known that vortex flow in tubes can enhance the single-phase heat transfer coefficient and extend the critical heat flux (CHF) (departure from nucleate boiling) in subcooled boiling by about a factor of 2 over the corresponding straight flow values for conditions under which the tubes are uniformly heated in circumference and length.[2] The correlation for CHF derived by Gambill[2] from the data under such conditions is based on a heated-length argument. Application of this correlation to particle beam targets illuminated only on a single side results in underestimates of the peak heat flux (CHF) capabilities of these devices. As pointed out by Kim,[3] circumferential heat conduction in the tube wall due to asymmetric heating would reduce the peak heat flux to the coolant on the illuminated side, but this could account for only about a 20% reduction over the uniformly heated case. For the most part, the large improvement in CHF is evidently due to the circulating flow pattern created by the twisted tape insert (see Fig. 1). The resulting large component of tangential velocity (78% of the axial value) creates a situation in which subcooled liquid is continuously swept past the heated side of the tube, as shown in Fig. 2. If we interpret the relevant scale length for the heat flux as the width of the hot patch, and not the heated length, then the latest ORNL results are not inconsistent with the results of Gambill. In this study, we concentrate on the effects of nonuniform heating as it relates to the data obtained from the calorimeter installed on the METF neutral beam test stand. The swirl tube is modeled with a two-dimensional (2-D), unsteady heat conduction code that includes a temperature dependence for the heat transfer coefficients in forced convective subcooled boiling and temperature-dependent physical properties.

The numerical results determine, in addition to the heat flux capabilities of the swirl tube, the temporal response of the tube, swirl flow heat transfer coefficients, and temperature profiles from which thermal stress calculations can be made. Potential fusion applications such as plasma limiters and other high-heat-flux plasma-side components are discussed briefly.

ORNL PHOTO 7015-84

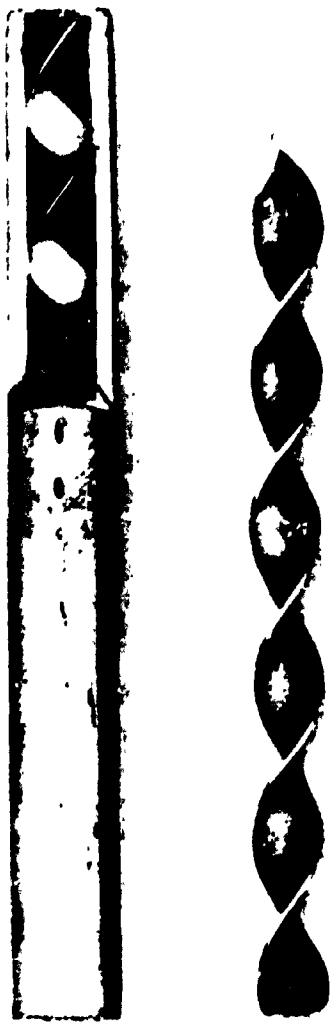

Fig. 1. Photograph of swirl tube showing twisted tape insert.

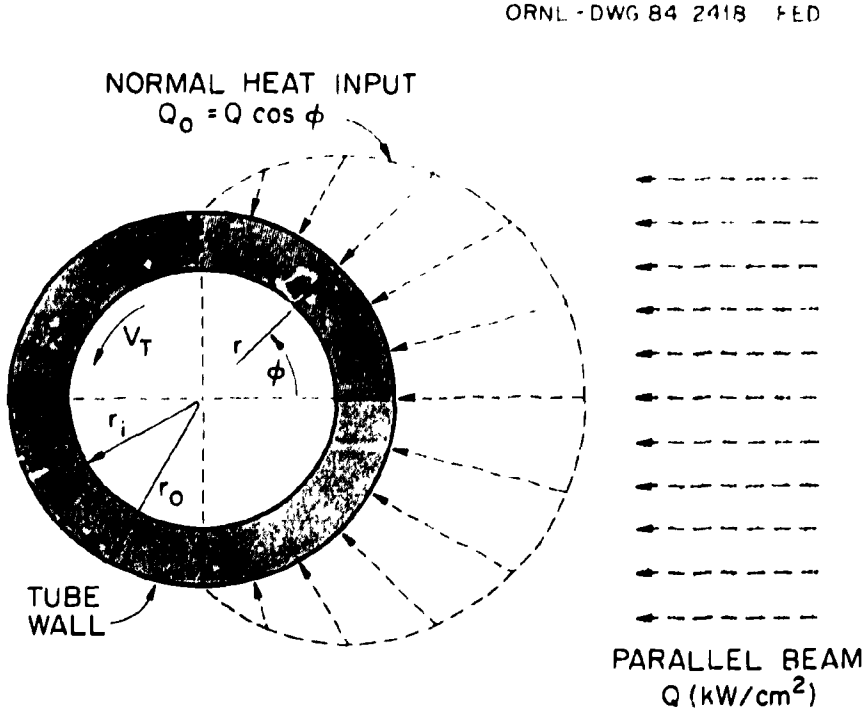

Fig. 2. Schematic representation of swirl flow heat transfer showing tangential flow component and normal heat flux distribution for single-sided particle beam illumination.

2. DESCRIPTION OF THE MODEL

2.1 EXPERIMENTAL CONDITIONS

The pertinent details of the experiment on which the model is based are summarized in Fig. 3 and Table 1. The apex of the calorimeter is located 640 cm from the ion source. The beam at that point is approximately Gaussian in shape with a maximum power density on axis of $\approx$15 kW/cm^2 and a half-width at half-maximum of $\approx$7 cm.

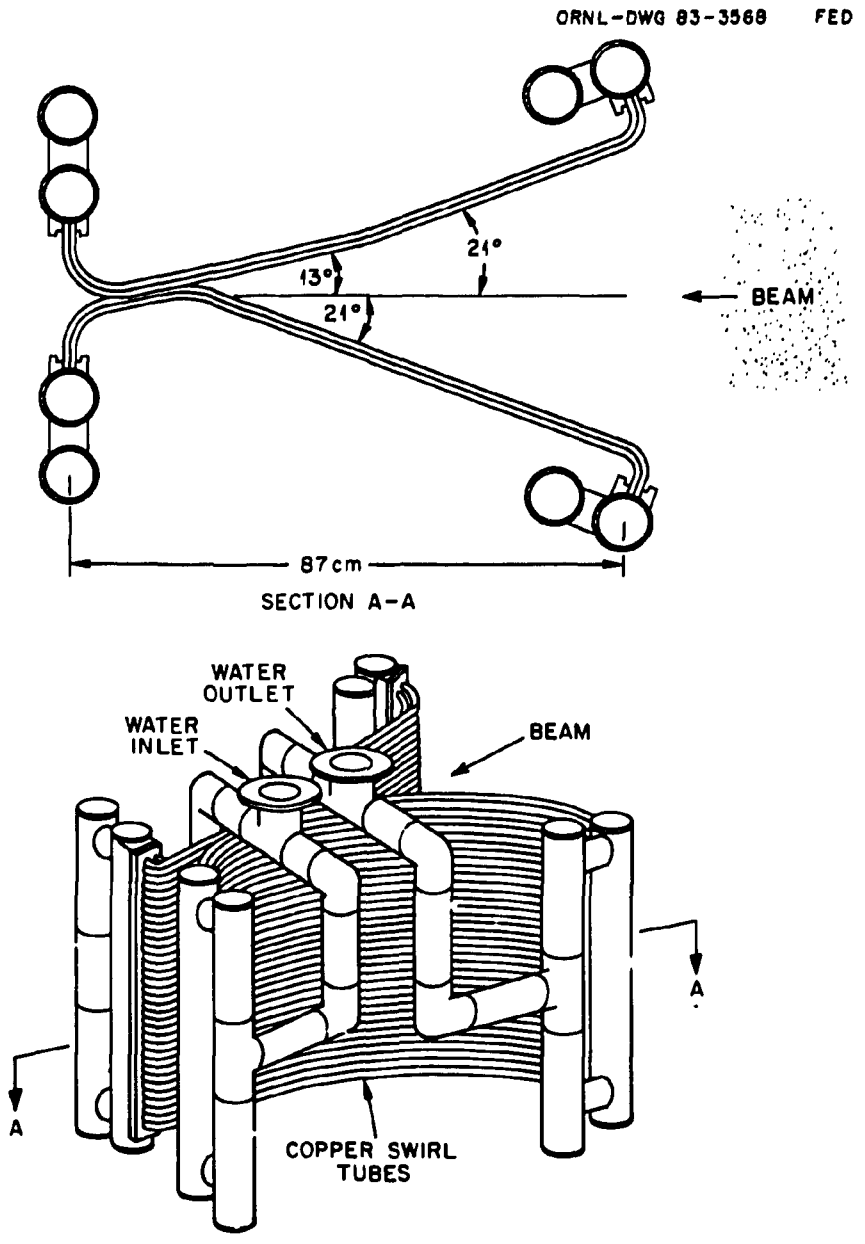

Fig. 3. Schematic of the METF swirl tube neutral beam target.

Table 1. Maximum test parameters for METF swirl tube neutral beam target

Test location: ORNL Medium Energy Test Facility
Power source: ORNL long-pulse ion source
Target: 126 inclined water-cooled copper swirl tubes

Source voltage, kV	75
Source current, A	40
Pulse length, s	30
Extracted power, MW	3
Extraction surface, cm	13.2 × 43.7
Focal length, cm	950
Power density at 640 cm downstream, kW/cm^2	≈15
Swirl tube outside diameter, cm	0.95
Swirl tube wall thickness, cm	0.16
Angle α between tube arrays and beam axis, deg	13 and 21
Water flow rate, L/s (gpm)	
Total	41.6 (660)
Average per tube	0.33 (5.2)
Water velocity, m/s	11.6
Water pressure, MPa (psia)	
Inlet	1.45 (210)
Outlet	0.31 (45)
Temperature difference ΔT, °C	15.7
Measured power, MW	2.7
Tube surface heat flux, kW/cm^2	≈5.4

The axis of each tube is inclined at an angle of 21° with respect to the beam, which produces a power flux normal to the plane of the tubes of 5.4 kW/cm^2 and a half-width projected onto the tube length of 17 cm. The numerical results are based on these values; the 2-D model neglects heat conduction along the length of the tube.

The tests were performed at a water flow rate of 0.33 L/s (5 gpm) per tube and a corresponding axial velocity of 1160 cm/s. The tape twist ratio, which is defined as the number of internal diameters for 180° of twist, is 2. This translates into values for the resultant and tangential velocities at the inside wall of 1470 cm/s and 900 cm/s, respectively. The pressure drop associated with this flow is 11.2 bar (165 psi). The pressure at the apex is estimated to be 10.2 bar (150 psia), for which the saturation temperature T_{sat} is 175°C.

The tube material is OFHC copper. The diameter is 0.95 cm (0.375 in.), and the wall thickness is 0.16 cm (0.0625 in.).

2.2 TWO-PHASE FLOW HEAT TRANSFER

The heat transfer at the metal-water interface is characterized by forced convective subcooled boiling at the illuminated side and liquid, single-phase, forced convection on the opposing surface. Consequently, the heat transfer coefficient is nonuniform, and, in order to account for the nonlinear variation around the circumference, a composite coefficient was constructed according to the additive method of Bergles and Rohsenow.[4] The heat flux to the fluid Q_w is determined from the single-phase forced convective flux Q_{FC}, from the fully developed subcooled boiling heat flux Q_{SCB} as determined by the instantaneous

wall temperature, and from conditions corresponding to the onset of nucleate boiling Q_{ONB} from the following relationship:

$$Q_w = Q_{FC}\left\{1 + \left[\frac{Q_{SCB}}{Q_{FC}}\left[1 - \frac{Q_{ONB}}{Q_{SCB}}\right]\right]^2\right\}^{1/2} . \quad (1)$$

The swirl flow correlation of Gambill[2] was chosen for the single-phase heat transfer coefficient. It is a modified form of the Dittus-Boelter equation that gives values roughly a factor of 2 larger than the well-known straight flow correlation. The heat transfer coefficient h_{FC} is given by

$$\frac{h_{FC}}{C_{pf}G_a} = 0.05\left[1 + \left(\frac{D_i}{L_H}\right)^{0.7}\right] y^{-0.09}\mathrm{Re}^{-0.2}\mathrm{Pr}^{-2/3} , \quad (2)$$

where C_{pf} (J/g) is the specific heat of water, D_i is the internal diameter of the tube, L_H is the heated length, y is the tape twist ratio, and Pr is the Prandtl number. The mass flux G_a (g/cm^2) and the Reynolds number Re are based on the axial flow component. For our conditions, the heated length is very much larger than the internal diameter, and consequently the term involving L_H is small. The single-phase heat flux is determined from the fluid temperature T_F and local temperature of the inside wall T_w by

$$Q_{FC} = h_{FC}(T_w - T_F) . \quad (3)$$

The correlation of Thom et al.[5] is used for the fully developed subcooled boiling heat flux. It is expressed in terms of the inside wall temperature T_w, the saturation temperature T_{sat}, and the pressure P (bar) of the fluid as

$$Q_{SCB}(T_w) = 0.197[(T_w - T_{sat})\exp(P/87)]^2 \quad (4)$$

(in watts per square centimeter). The temperature of the wall T_{ONB} at which the onset of nucleate boiling occurs is determined by the method of Bergles and Rohsenow.[4] Incipient boiling commences when the forced convective heat flux equals a minimum value given by

$$h_{FC}(T_{ONB} - T_F) = 1099\,P^{1.156}[1.8(T_{ONB} - T_{sat})]\exp(2.16/P^{0.0234}) . \quad (5)$$

The value of T_{ONB} found in this way is substituted for T_w in Eq. (4) to obtain the contribution Q_{ONB} to Eq. (1).

The resultant heat flux from Eq. (1) is plotted in Fig. 4 as a function of the wall superheat $\Delta T_{sat} = T_w - T_{sat}$. The data of Gambill for comparable tape twist ratios are presented for comparison. The agreement is good, although Gambill's measurements cover only a limited range of the boiling curve and apparently do not extend into the fully developed boiling regime where most of our results apply.

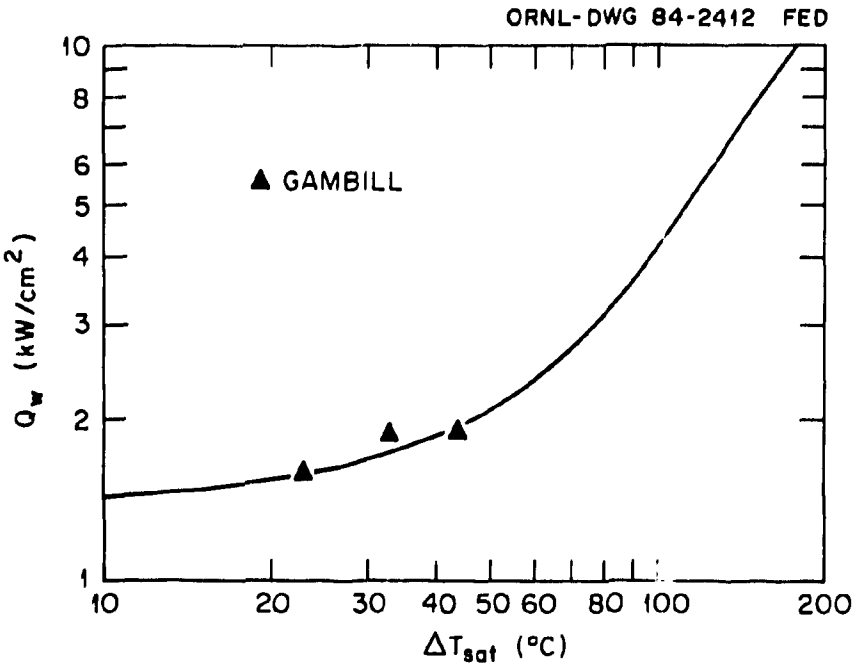

Fig. 4. Forced convective subcooled boiling curve calculated from Eq. (1) compared with the data of Gambill.[3]

2.3 HEAT CONDUCTION

The evolution of the temperature in the tube wall is governed by the unsteady heat conduction equation in cylindrical coordinates,

$$\rho \frac{\partial C_p T}{\partial t} = \frac{1}{r}\frac{\partial}{\partial r}\left[rk\,\frac{\partial T}{\partial r}\right] + \frac{1}{r^2}\frac{\partial}{\partial \phi}\left[k\,\frac{\partial T}{\partial \phi}\right] , \tag{6}$$

where ρ is the mass density, C_p is the specific heat, and k is the thermal conductivity. In this formulation, the physical properties are allowed to have a temperature dependence.

Equation (6) was solved by the method of finite differences, subject to the following boundary conditions at the outer and inner radii:

$$k\frac{\partial T}{\partial r} = \begin{cases} Q_0(\phi,t) & \text{at} \quad r = r_0 \\ Q_w(T_w) & \text{at} \quad r = r_i \end{cases} ,$$

where $Q_0(\phi,t)$ is the prescribed incident heat flux (normal to the tube surface) and $Q_w(T_w)$ is the heat transfer at the inner wall as determined from T_w by Eq. (1). For the initial condition, the temperature is taken everywhere to be equal to the coolant temperature $T_F = 20°C$.

3. RESULTS

The numerical results for the conditions corresponding to the METF calorimeter tests are presented in Figs. 5 and 6 for the peak power conditions. In Fig. 5, the steady-state wall heat flux and heat transfer coefficient h are shown for a copper tube subject to an incident power flux of 5.4 kW/cm^2. The heat flux calculated for the uniformly heated case at the same intensity is presented for comparison. Lateral heat conduction is responsible for reducing the heat flux to the water on the midplane from 8 kW/cm^2 to 7 kW/cm^2, but the sharp decrease of Q_w with ϕ is due primarily to the cos ϕ dependence of the incident heat flux. The heat transfer coefficient at the coolant interface varies by approximately a factor of 3 and is characterized by boiling over the entire illuminated side and single-phase convection on the opposing surface. For these conditions, boiling does not occur until the heat flux exceeds ≈1.5 kW/cm^2.

The temporal response of the swirl tube to a front-surface heat pulse of 5.4 kW/cm^2 is illustrated in Fig. 6. The inner wall heat flux at the midplane reaches 90% of its equilibrium value in less than 100 ms. The rapid response is due to the high thermal conductance across the tube wall, which is matched effectively by the heat removal capability at the coolant interface [Biot number $= h(r_0 - r_i)/k \approx 1$]. The rear surface responds more slowly because of the longer conduction path and lower heat transfer coefficients.

The rapid thermal response means that the tubes will experience a full thermal stress cycle for pulses as short as 100 ms. As mentioned earlier, the METF calorimeter has

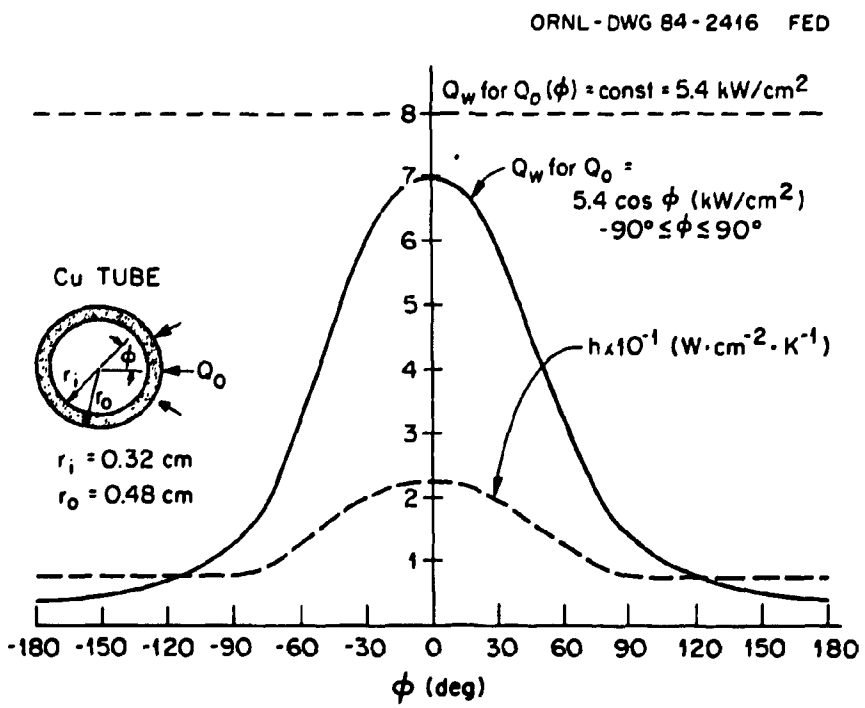

Fig. 5. Calculation of the inner wall steady-state heat flux distribution for uniform (dashed line) and single-sided (solid line) illumination at 5.4 kW/cm^2. The heat transfer coefficient for the latter is presented.

ORNL-DWG 84-2417 FED

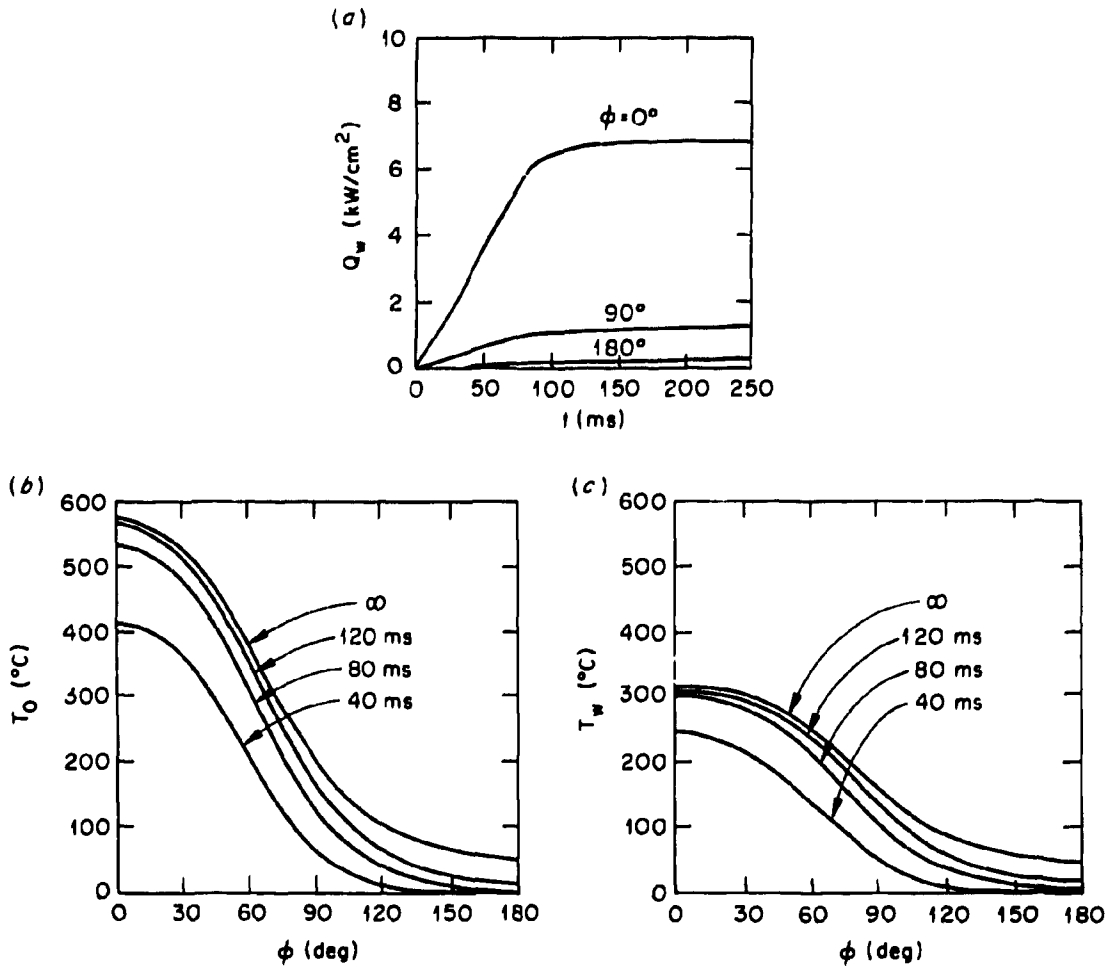

Fig. 6. Temporal response of a copper tube to an incident neutral beam pulse of 5.4 kW/cm^2 applied at $t = 0$. (a) Inner wall heat flux at three azimuthal locations. (' ` Temperature profile evolution at the exposed surface. (c) Temperature profile evolution at the cooled surface.

been subjected to ≈25,000 full-power pulses that were longer than this. A complete thermal stress analysis for this case was not performed, but to obtain an estimate of the magnitude of the cyclic stresses, a thermoelastic calculation was made for the temperature distributions shown in Fig. 6, assuming that the temperature does not vary along the length of the tube. In this approximation, the peak circumferential stress occurs at the inner wall midplane position on the side exposed to the beam. This stress is tensile with a magnitude of 197 MPa (29,000 psi); the corresponding value on the opposing cold surface is 68 MPa (10,000 psi). Although plastic deformation is expected under these conditions, mechanical failure or evidence of surface damage associated with thermal fatigue was not observed during the course of the METF tests.

As mentioned earlier, the peak calculated heat flux shown in Fig. 5 is greater than the corresponding CHF reported by Gambill for tubes that are heated uniformly over the

circumference and length. For such conditions, Gambill correlated CHF with the resultant inner wall velocity V_r and the heated length according to

$$Q_{CHF} = 0.473 + 0.0035\, V_r \left(\frac{L_H}{D_i}\right)^{-1/3} \tag{7}$$

(in kilowatts per square centimeter), where V_r is determined from the axial velocity V and the tape twist ratio,

$$V_r = 0.5 \frac{V}{y} (4y^2 + \pi^2)^{1/2} \tag{8}$$

(in centimeters per second). This relationship is plotted in Fig. 7 for values of V_r and y corresponding to the METF target. For heated lengths on the order of the beam

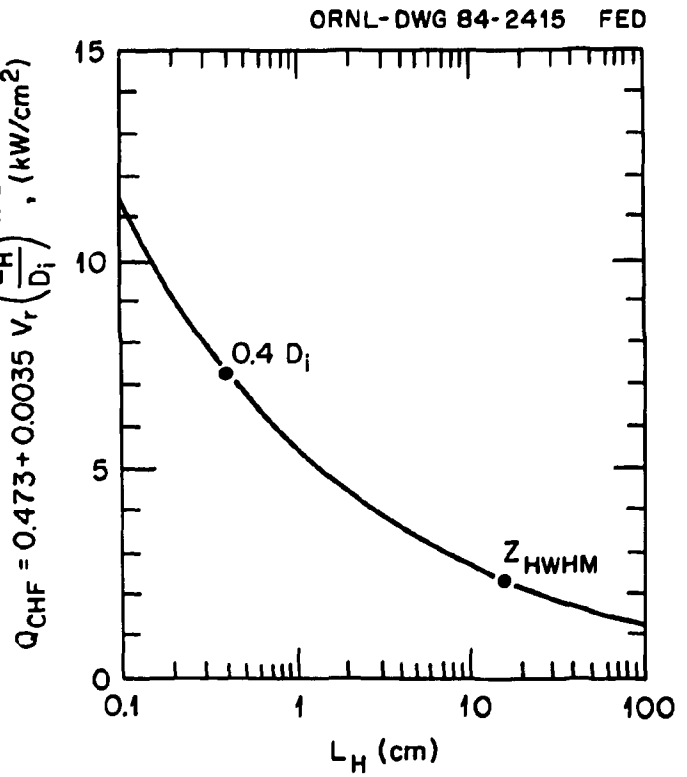

Fig. 7. Gambill's correlation of the critical heat flux with heated length for a uniformly heated tube. The point labeled Z_{HWHM} corresponds to the half-width of the METF beam power profile projected on the axis of the calorimeter tube. The calorimeter absorbs a heat flux at the innerwall midplane position of 7 kW/cm^2, which corresponds to the point labeled $0.4D_i$, where D_i is the internal diameter.

half-width (projected onto the length of the tube), the correlation predicts burnout at 2.5 kW/cm^2 for a uniformly heated tube. The average of the heat flux over the entire circumference of the METF target is not much larger than this value, but the numerical results show that the heat flux exceeds the prediction locally over nearly half the tube circumference. The length scale that corresponds to the peak calculated heat flux of 7 kW/cm^2 is 0.26 cm, which is characteristic of the lateral size of the hot patch. This suggests a correlation that is based not on the heated length but on the tube diameter. The basis for this interpretation is the observation that, for highly asymmetric heating, the vortex flow pattern provides the boiling interface with a continuous supply of subcooled liquid. If the heat input is small enough to ensure that the bulk fluid remains in the subcooled state, this condition should apply everywhere along the length of the tube. According to this argument, the heated length should not be a factor in the determination of the CHF.

Since burnout conditions were not observed in any of the previous tests, this theory is untested. Moreover, the full potential of swirl tubes has not been determined for this heating configuration.

4. CONCLUSIONS

The extensive tests performed on the METF neutral beam target and the numerical results presented here have demonstrated the potential of swirl flow heat transfer for applications with highly asymmetric heating profiles. In this configuration, the heat extraction capability is at least a factor of 2 greater than the CHF value reported by Gambill for uniformly heated tubes. When compared to straight flow conditions, the performance is yet another factor of 2 higher.

Besides particle beam targets, there are numerous potential applications for swirl tube heat removal technology in fusion engineering, including plasma limiters, divertor collector plates, rf launchers, and Faraday shields. These plasma-side components will experience heating mechanisms similar to those affecting beam stops, but the particle energies will typically be much smaller. Long-pulse magnetic confinement devices based on the tokamak, stellarator, and mirror concepts will require active cooling to operate at steady state. Although the heat loads can in principle be kept at manageable levels by design, localized heating and off-normal operating conditions, such as those encountered during plasma disruptions, may be unavoidable. In this regard, the plasma limiter presents the most demanding design challenge. The limiter must be able to absorb the steady-state plasma heat conduction losses and withstand the more extreme plasma energy dump during a disruption. The relative importance of these two functions depends for the most part on the relative magnitude of the energy confinement time τ_E and the time duration of the disruption τ_D. If τ_E is large in comparison to τ_D, then sufficient surface area must be incorporated in the design to limit the surface temperature rise during the disruption transient. For these conditions the large-area limiter is only lightly loaded at the normal operating point. When the disruption time lengthens in comparison to τ_E, then the disruption heat flux becomes more manageable, and a more compact design and concomitant higher steady-state heat flux capability result. Examples of both cases are shown in Figs. 8 and 9 for a uniform heat flux limiter design. The conditions corresponding to the calculation of Fig. 8 are estimates for the Tokamak Fusion Test Reactor (TFTR) during $Q = 1$ operation with 27.5 MW of input power, 70% heat conduction loss, $\tau_E = 0.25$ s, and $\tau_D = 0.002$ s (ref. 6). Molybdenum was chosen as the tube material, and a surface area of 3.8×10^4 cm^2 was specified to limit the temperature of the outer surface midplane position to $\approx$1700°C during the disruption. This results in a steady-state incident heat flux of 500 W/cm^2. During the transient, the thermal response is inertial. The heat flux at the inside wall reaches its peak value of 2.6 kW/cm^2 about 15 ms after termination of the 62.5-kW/cm^2 disruption heat pulse. The equilibrium is reestablished in $\approx$300 ms. This state is characterized by low system temperatures, single-phase heat transfer, and a heat flux that is high by most standards but modest in comparison to the heat removal capability of the swirl tube. For this application, a thicker tube wall could be substituted without substantially altering the performance (a 3-mm wall will raise the peak temperatures by 120°C).

The results of a calculation for conditions that are typical of an Impurity Study Experiment (ISX-B) neutral-beam-heated discharge are presented in Fig. 9. The disruption time of 1 ms is comparable to the TFTR example, but the energy confinement time of 15 ms is substantially smaller. The energy stored in the plasma is proportionally much

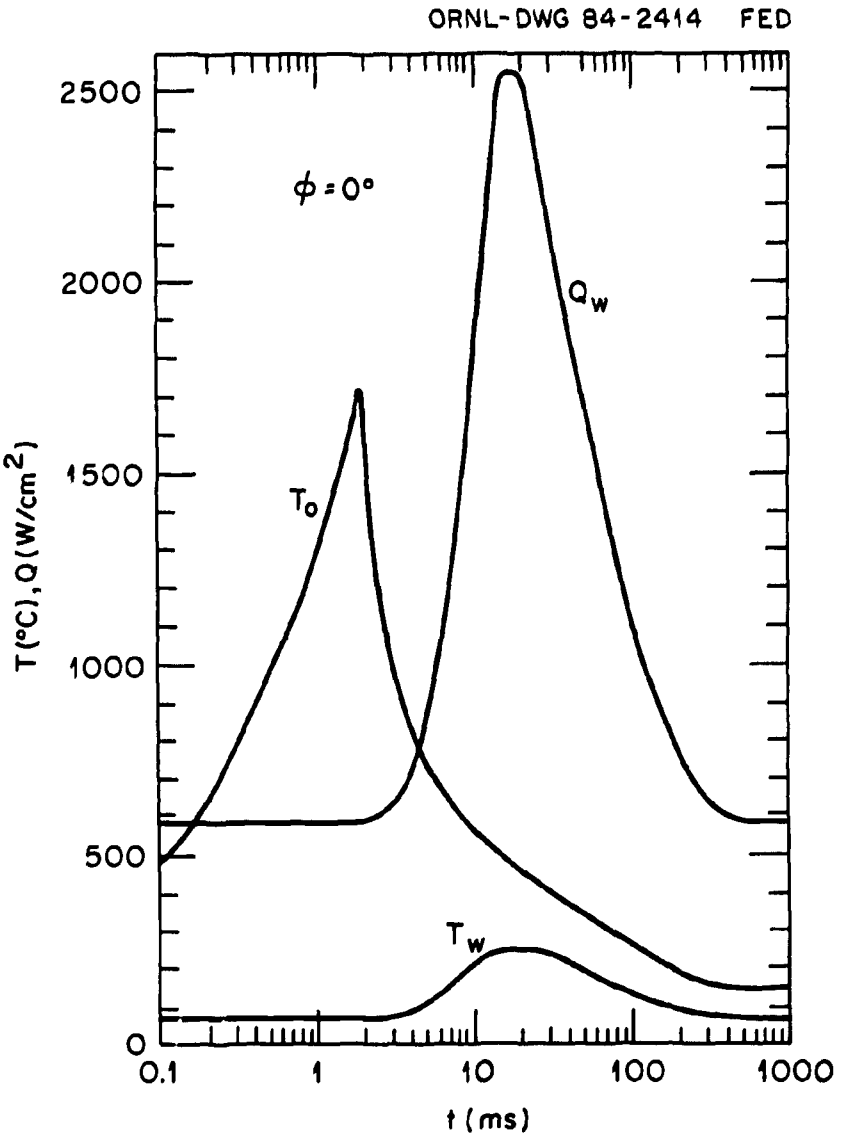

Fig. 8. Midplane conditions of a molybdenum tube in response to a 62.5-kW/cm² heat pulse lasting 2 ms superposed on a constant background heat load of 0.5 kW/cm². T_0 = exposed surface temperature, T_w = inside wall temperature, Q_w = inner wall heat flux.

smaller than in the previous example; consequently, a more compact limiter design (4.0×10^2 cm^2) will accommodate the disruption heat load. The response to the transient is similar to that in the previous example, but the background conditions are elevated substantially because of the small area. The steady-state incident heat flux is 3.5 kW/cm^2, which is beyond the capability of unaugmented water-cooled heat transfer but comfortably within the range of swirl flow heat removal technology.

A plasma limiter based on tubular elements provides an inherent plasma exhaust or pumping capability for particle control. In the design illustrated in Fig. 10, the tubes

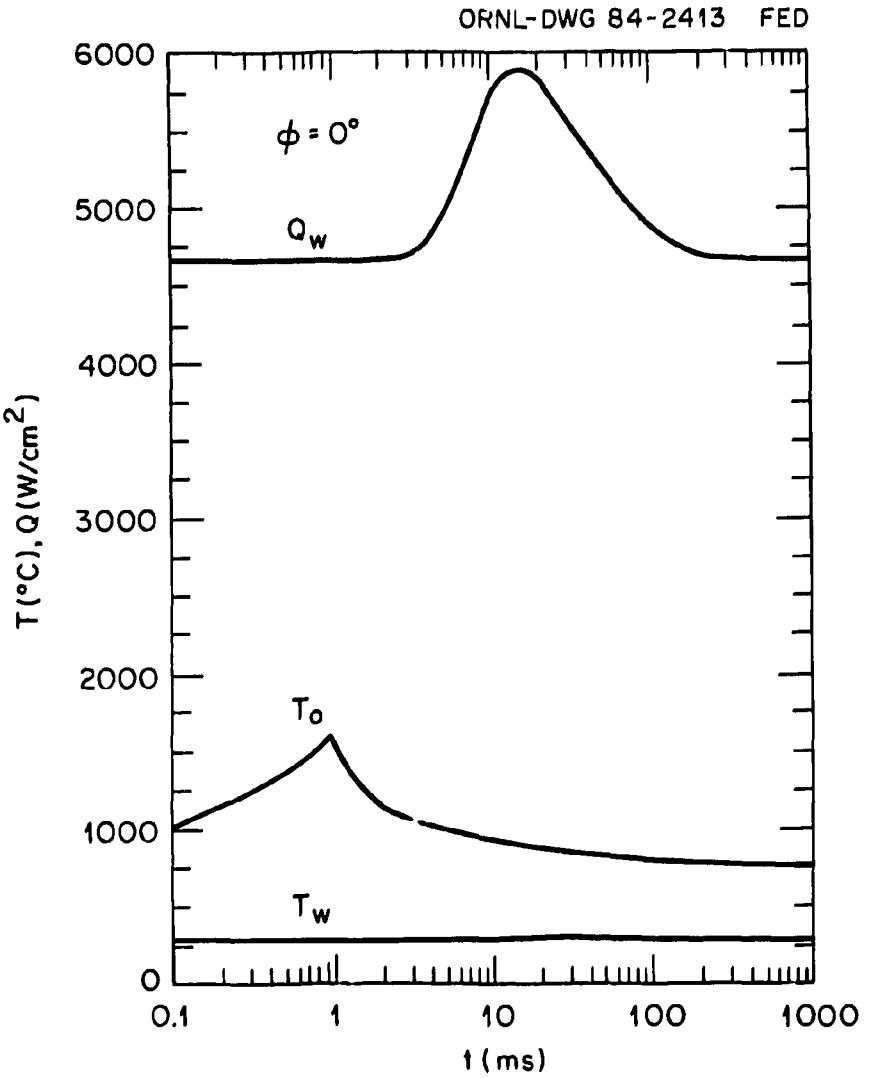

Fig. 9. Midplane conditions of a molybdenum tube in response to a 52.5-kW/cm^2 heat pulse lasting 1 ms superposed on a constant background heat load of 3.5 kW/cm^2. T_0 = exposed surface temperature, T_w = inside wall temperature, Q_w = inner wall heat flux.

would be aligned in a grillwork fashion along the magnetic field and shaped to form a uniform heat flux contour. Plasma and neutralized particles that escaped through the passages between the tubes would be collected in a duct or chamber behind the limiter blade by cryopumps or getter panels. This configuration would probably be most effective at collecting the neutral particles formed during dissociation of the molecular hydrogen desorbed from the surface of the tubes in contact with the plasma. The high heat transfer of the swirl tubes would provide a desirable safety margin against uncertainties in the plasma scrapeoff layer. Because of its compactness and simple construction, the limiter assembly should be inexpensive. The use of active cooling and the fast thermal response

ORNL-DWG 84-2649 FED

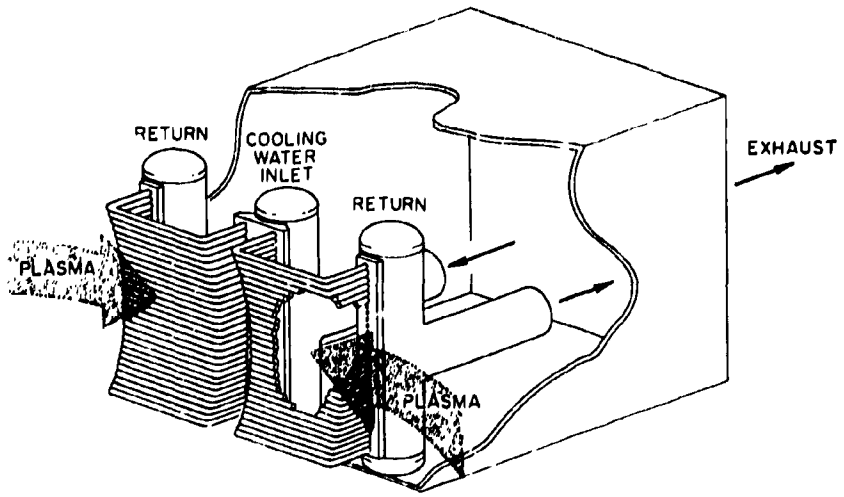

Fig. 10. Design of a pump limiter module based on swirl tube elements. The partial transparency of the grillwork limiter blades allows particles to enter the pump duct.

provide a simple calorimeter for measurement of the instantaneous plasma heat conduction loss.

Some aspects of this concept that require further study include analysis of the plasma exhaust efficiency of the tube bank, a calculation of the cyclic thermal stresses, thermal fatigue lifetime measurements, and evaluation of the applicability of low-Z coatings or claddings to eliminate contamination of the plasma with high-Z impurities.

17/18

REFERENCES

1. S. K. Combs et al., "Development of a High-Heat-Flux Target for Multimegawatt, Multisecond Neutral Beams at ORNL," p. 583 in *Proceedings of the 10th Symposium on Fusion Engineering*, Vol. 1, Institute Electrical and Electronics Engineers, New York, 1983.

2. W. R. Gambill, R. D. Bundy, and R. W. Wansbrough, "Heat Transfer, Burnout and Pressure Drop for Water in Swirl Flow Through Tubes with Internal Twisted Tapes," *Chem. Eng. Prog.* **57** (32), 127–37 (1961), cited in W. M. Rohsenow and J. P. Hartnett, *Handbook of Heat Transfer*, McGraw-Hill, New York, 1973.

3. J. Kim et al., "A Heat Transfer Study of Water-Cooled Swirl Tubes for Neutral Beam Targets," pp. 85–94 in *Proceedings of the Seventh Symposium on Engineering Problems of Fusion Research*, Institute Electrical and Electronics Engineers, New York, 1977.

4. A. E. Bergles and W. M. Rohsenow, "The Determination of Forced Convection Surface Boiling Heat Transfer," paper 63-HT-22 presented at the 6th National Heat Transfer Conference of the ASME-AIChE, Boston, August 11–14, 1963, cited in J. G. Collier, *Convective Boiling and Condensation*, McGraw-Hill, London, 1972.

5. J. R. S. Thom et al., "Boiling in Subcooled Water During Flow Up Heated Tubes or Annuli," paper presented at the Symposium on Boiling Heat Transfer in Steam Generating Units and Heat Exchangers, Manchester, England, September 15–16, 1965, cited in J. G. Collier, *Convective Boiling and Condensation*, McGraw-Hill, London, 1972.

6. M. Ulrickson, Princeton Plasma Physics Laboratory, Princeton, N.J., private communication, Feb. 23, 1984.

ORNL/TM-9183
Dist. Category UC-20

INTERNAL DISTRIBUTION

1. D. R. Baumgardner
2. W. L. Gardner
3. M. M. Menon
4. W. L. Stirling
5. J. Sheffield
6. L. A. Berry
7. J. L. Dunlap
8. M. J. Saltmarsh
9. J. R. Haines
10–14. S. L. Milora
15–19. S. K. Combs
20–24. C. A. Foster
25–26. Laboratory Records Department
27. Laboratory Records, ORNL-RC
28. Central Research Library
29. Document Reference Section
30. Fusion Energy Division Library
31. Fusion Energy Division Publications Office
32. ORNL Patent Office

EXTERNAL DISTRIBUTION

33. Office of the Assistant Manager for Energy Research and Development, Department of Energy, Oak Ridge Operations, Box E, Oak Ridge, TN 37831
34. J. D. Callen, Department of Nuclear Engineering, University of Wisconsin, Madison, WI 53706
35. R. W. Conn, Department of Chemical, Nuclear, and Thermal Engineering, University of California, Los Angeles, CA 90024
36. S. O. Dean, Director, Fusion Energy Development, Science Applications, Inc., 2 Professional Drive, Gaithersburg, MD 20760
37. H. K. Forsen, Bechtel Group, Inc., Research Engineering, P.O. Box 3965, San Francisco, CA 94105
38. R. W. Gould, Department of Applied Physics, California Institute of Technology, Pasadena, CA 91125
39. D. G. McAlees, Exxon Nuclear Company, Inc., 777 106th Avenue, NE, Bellevue, WA 98009
40. P. J. Reardon, Princeton Plasma Physics Laboratory, P.O. Box 451, Princeton, NJ 08544
41. W. M. Stacey, Jr., School of Nuclear Engineering, Georgia Institute of Technology, Atlanta, GA 30332
42. G. A. Eliseev, I. V. Kurchatov Institute of Atomic Energy, P.O. Box 3402, 123182 Moscow, U.S.S.R.

43. V. A. Glukhikh, Scientific-Research Institute of Electro-Physical Apparatus, 188631 Leningrad, U.S.S.R.
44. I. Spighel, Lebedev Physical Institute, Leninsky Prospect 53, 117924 Moscow, U.S.S.R.
45. D. D. Ryutov, Institute of Nuclear Physics, Siberian Branch of the Academy of Sciences of the U.S.S.R., Sovetskaya St. 5, 630090 Novosibirsk, U.S.S.R.
46. V. T. Tolok, Kharkov Physical-Technical Institute, Academical St. 1, 310108 Kharkov, U.S.S.R.
47. R. Varma, Physical Research Laboratory, Navrangpura, Ahmedabad, India
48. Bibliothek, Max-Planck-Institut fur Plasmaphysik, D-8046 Garching bei Munchen, Federal Republic of Germany
49. Bibliothek, Institut fur Plasmaphysik, KFA, Postfach 1913, D-5170 Julich, Federal Republic of Germany
50. Bibliotheque, Centre de Recherches en Physique des Plasmas, 21 Avenue des Bains, 1007 Lausanne, Switzerland
51. Bibliotheque, Service du Confinement des Plasmas, CEA, B.P. 6, 92 Fontenay-aux-Roses (Seine), France
52. Documentation S.I.G.N., Departement de la Physique du Plasma et de la Fusion Controlee, Centre d'Etudes Nucleaires, B.P. No. 85, Centre du Tri, 38041 Cedex, Grenoble, France
53. Library, Culham Laboratory, UKAEA, Abingdon, Oxfordshire, OX14 3DB, England
54. Library, FOM Instituut voor Plasma-Fysica, Rijnhuizen, Jutphaas, The Netherlands
55. Library, Institute of Physics, Academia Sinica, Beijing, Peoples Republic of China
56. Library, Institute of Plasma Physics, Nagoya University, Nagoya
57. Library, International Centre for Theoretical Physics, Trieste, Italy
58. Library, Laboratorio Gas Ionizzati, Frascati, Italy
59. Library, Plasma Physics Laboratory, Kyoto University, Gokasho Uji, Kyoto, Japan
60. Plasma Research Laboratory, Australian National University, P.O. Box 4, Canberra, A.C.T. 2000, Australia
61. Thermonuclear Library, Japan Atomic Energy Research Institute, Tokai, Naka, Ibaraki, Japan
62. T. V. George, Office of Fusion Energy, Office of Energy Research, Mail Station G-256, U.S. Department of Energy, Washington, DC 20545
63. G. M. Haas, Office of Fusion Energy, Office of Energy Research, Mail Station G-256, U.S. Department of Energy, Washington, DC 20545
64. E. Oktay, Office of Fusion Energy, Office of Energy Research, Mail Station G-256, U.S. Department of Energy, Washington, DC 20545

65. H. S. Staten, Office of Fusion Energy, Office of Energy Research, Mail Station G-256, U.S. Department of Energy, Washington, DC 20545

66–171. Given distribution as shown in TID-4500 Magnetic Fusion Energy (Category Distribution UC-20)